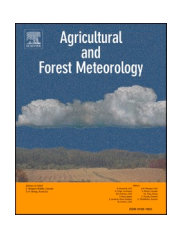
ELSEVIER

Contents lists available at ScienceDirect

Agricultural and Forest Meteorology

journal homepage: www.elsevier.com/locate/agrformet





Estimating root zone soil moisture across diverse land cover types by integrating in-situ and remotely sensed data

Briana M. Wyatt a,*, Tyson E. Ochsner b, Chris B. Zou c

- a Department of Soil and Crop Sciences. Texas A&M University. 2474 TAMU. College Station. TX 77843. United States
- b Department of Plant and Soil Sciences, Oklahoma State University, 371 Agricultural Hall, Stillwater, OK 74078, United States
- ^c Department of Natural Resource Ecology and Management, Oklahoma State University, 008C Agricultural Hall, Stillwater, OK 74078, United States

ARTICLE INFO

Keywords: Soil moisture Remote sensing Land cover MODIS

ABSTRACT

Many soil moisture networks monitor only one land cover type, typically grassland, and the availability of in-situ soil moisture data in other land cover types is severely limited. Satellite-based radiometers lack adequate resolution to match the spatial variability in land cover, which often occurs at the sub-kilometer scale. Thus, spatial and temporal dynamics of root zone soil moisture in regions with heterogeneous land cover types remain poorly understood. Our objective was to determine how effectively root-zone soil moisture for diverse land cover types can be estimated using a water balance model driven by normalized high-resolution, remotely sensed vegetation indices (VI) data and in-situ meteorological data. Root zone soil moisture dynamics under four different land cover types were estimated using normalized VI data as a proxy for the basal crop coefficient. Correlation coefficients (*r*) between measured and modeled soil moisture ranged from 0.50–0.92, mean absolute error (MAE) ranged from 0.03–0.06 m³ m⁻³, and mean bias error (MBE) ranged from -0.05–0.02 m³ m⁻³ across tallgrass prairie, cropland, mixed hardwood forest, and loblolly pine plantation sites. Model-estimated soil moisture under each land cover type was more accurate than both measured data from the nearest long-term grassland monitoring site and data from the NASA-USDA Enhanced Soil Moisture Active-Passive (SMAP) soil moisture product, providing evidence that in-situ meteorological data and remotely sensed VI data may be integrated into a simple water balance model to better estimate root zone soil moisture across diverse land cover types.

1. Introduction

Soil moisture is an essential climate variable affecting near-surface temperature, hydrological processes, agricultural production, and the health of ecological systems (Ochsner et al., 2013; Wagner et al., 2007; Wagner et al., 2012). Soil moisture data from in-situ monitoring networks have been used to estimate deep drainage (Zhang et al., 2019; Wyatt et al., 2017), improve streamflow forecasts (Wyatt et al., 2020; Harpold et al., 2017), and improve agronomic decision making (Lollato et al., 2016; Lollato et al., 2018). However, the majority of soil moisture data currently available from in-situ monitoring networks reflect conditions under a single land cover type, typically grassland; however soil water conditions under other nearby land cover types, such as croplands or forests, may differ significantly from these measured values (Zou et al., 2014; Patrignani and Ochsner, 2018).

Unlike in-situ data, remotely sensed soil moisture products from satellites can provide global data that capture spatial and temporal

variations in soil moisture across numerous land cover types (Mohanty et al., 2017). However, these data suffer from several limitations, including a shallow sensing depth (\sim 5 cm), relatively coarse spatial resolution, and a limited ability to sense soil moisture under dense vegetation types such as forests (Mohanty et al., 2017; Peng et al., 2017; Kerr et al., 2001). The most accurate satellite soil moisture products are based on radiometers, which have footprints of >30 km (Entekhabi et al., 2010). Because vegetation types are often intermixed at smaller scales (< 1 km), variations in soil moisture caused by contrasting land cover types are not adequately captured by current remote-sensing soil moisture products.

A growing body of research shows the potential of higher resolution, remotely sensed vegetation index (VI) data, such as those from NASA's Moderate Resolution Imaging Spectroradiometer (MODIS) sensors, to close this gap in spatial scale and provide new insights into the effects of land cover type on soil moisture (Zhu et al., 2020; Olivera-Guerra et al., 2018; Battude et al., 2017; Sanchez et al., 2012; Sanchez et al., 2010).

E-mail address: briana.wyatt@tamu.edu (B.M. Wyatt).

^{*} Corresponding author.

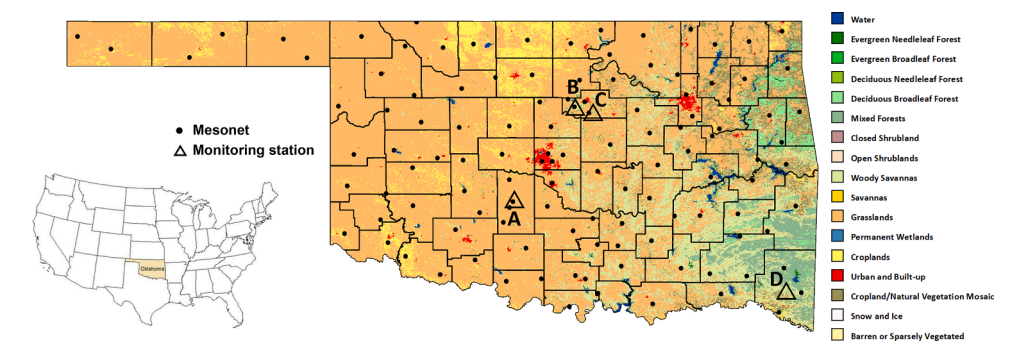


Fig. 1. Map of MODIS land cover types (500-m resolution) and county boundaries in Oklahoma, active Oklahoma Mesonet locations (black dots), and locations of independent soil moisture monitoring stations under various land cover types (triangles). Site A is a cropland, Site B is a tallgrass prairie, Site C is a hardwood forest, and Site D is a loblolly pine planation.

The concept of using remotely sensed VI data in mechanistic water and surface energy balance models has been frequently discussed in the literature (Hendrickx et al., 2016; Glenn et al., 2011; Glenn et al., 2010; Gonzalez-Dugo et al., 2009; Glenn et al., 2007), but most land surface models were not designed to incorporate these data. Incorporating new data types into existing mechanistic models may not improve model results (Ford and Quiring, 2013) and may actually decrease model performance due to overfitting issues (Transtrum and Qiu, 2016). Land surface models which are capable of integrating VI data, such as those within the North American Land Data Assimilation System (NLDAS), have a crude conceptual representation of soil characteristics, allow only monthly VI inputs, and have a maximum spatial resolution of ~1 km (Mitchell et al., 2004; Kumar et al., 2006).

The current research seeks to overcome the limitations presented by both in-situ and remotely sensed soil moisture data by integrating in-situ meteorological data and remotely sensed VI data into a simple water balance model based on the FAO-56 dual crop coefficient method (Allen

et al., 1998). This novel application, unlike most prior studies utilizing the FAO-56 water balance method, utilizes the model primarily to estimate daily root zone soil water content rather than evapotranspiration (ET). The resulting root zone soil moisture estimates are then evaluated against measured values at four independent in-situ monitoring locations under diverse land cover types. The goals of this research are: 1) to determine the suitability of using remotely sensed VI data as proxies for the basal crop coefficient in the water balance simulations of diverse land cover types, 2) to evaluate the accuracy of various approaches for computing crop coefficients from vegetation indices, and 3) to compare soil moisture estimates resulting from this water balance model under four different land cover types with a) measured values in each land cover type, b) data measured at nearby grassland monitoring stations, and c) root zone soil moisture data from the NASA-USDA SMAP soil moisture product.

This work presents an innovative method of integrating remote sensing VI data and measured meteorological data within the FAO-56

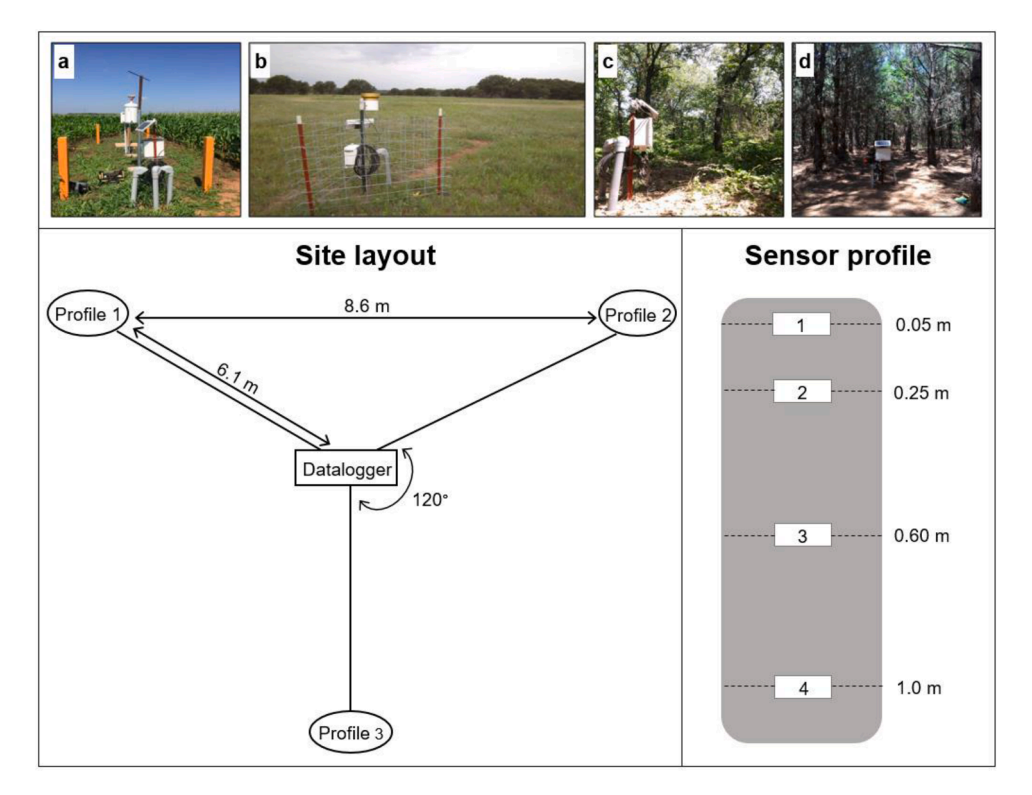


Fig. 2. Photos of the cropland (a), tallgrass prairie (b), hardwood forest (c), and loblolly pine plantation (d) sites; a diagram of the layout of monitoring sites A, C, and D; and an example soil moisture sensor profile of sites A, C, and D. Site B sensor profiles were farther apart with sensors at depths of 0.05, 0.10, 0.20, and 0.50 m below the surface.

Table 1 Geographic and long-term meteorological data for each site, including latitude and longitude, elevation above sea level, distance to the nearest Oklahoma Mesonet station, long-term mean daily maximum temperature (T_{min}), long-term mean annual precipitation (P), and the year in which soil moisture sensors were installed.

Site	Lat, Lon	Elevation	Distance to Mesonet	T_{max} , T_{min}	P	Year Installed
	deg.	m	km	°C	mm	
Loblolly Pine Plantation	34.03, -94.82	110	23.1	23.9, 11.0	1159	2019
Mixed Hardwood Forest	36.00, -97.04	292	1.00	22.3, 9.92	873	2018
Cropland	35.03, -97.91	328	0.13	23.1, 9.36	812	2018
Tallgrass Prairie	36.06, -97.21	327	0.47	22.1, 9.43	884	2012

model, and our results are among a small number of studies to show that this integration of data from different sources can lead to accurate estimates of root zone soil moisture under a wide variety of land cover types, including non-agricultural land cover types not traditionally considered within the FAO-56 model. To our knowledge, this study is the first conducted following the innovative work of Sanchez et al. (2010, 2012a, 2012b) which directly incorporates remote sensing VI data to estimate crop coefficients within the FAO-56 model without the inclusion of other additional input or calibration data. Further, the present study is the first application of this method in the U.S. and one of a few attempts to apply the FAO-56 model to estimate root zone soil moisture under non-agricultural land cover types.

2. Methods

2.1. Monitoring stations

Four locations in Oklahoma, USA, each with a different dominant land cover type, were chosen for modeling and as independent soil moisture monitoring locations to be used for model validation (Fig. 1). Land cover types at these sites include a mixed hardwood forest, a loblolly pine (Pinus taeda) plantation, rainfed (i.e., non-irrigated) cropland, and tallgrass prairie. At each monitoring location, arrays of soil moisture sensors (CS-655, Campbell Scientific, Inc., Logan, Utah) were installed in triplicate to monitor the volumetric water content in the soil profile. At the mixed hardwood forest, loblolly pine plantation, and cropland locations, soil moisture sensors were installed horizontally at depths of 5, 25, 60, and 100 cm. At these sites, sensor profiles were installed 6.1 m away from a central datalogger along headings separated by $\sim 120^{\circ}$ in order to maximize the distance between sensor profiles and reduce intercorrelation between soil moisture measurements (Fig. 2). Five-centimeter diameter soil cores with a length of 5.1 cm were taken horizontally adjacent to each sensor at the time of installation in each profile and at each depth (3 profiles per site \times 4 depths per profile = 12 cores per site).

At the tallgrass prairie location, CS-655 soil moisture sensors installed for a previous project were used. Sensors were installed in triplicate at this location as well, but farther apart than at the other three monitoring locations (mean of 449 m apart). At each tallgrass prairie monitoring profile, sensors were installed horizontally at 5, 10, 20, and 50 cm below the surface. As at the other sites, soil cores were collected from all soil profiles at the time of sensor installation. Soil cores from all sites were analyzed to estimate the soil volumetric water content at field capacity (-10 kPa, θ_{-10}) [m³ m⁻³], water content at wilting point (-1500 kPa, θ_{-1500}) [m³ m⁻³], bulk density [kg m⁻³], and fractions of sand, silt, and clay.

Measurements of soil apparent dielectric permittivity (K_a) [-], and electrical conductivity (EC) [dS m $^{-1}$] were collected either every hour (tallgrass prairie sites) or half hour (all other sites) using the CS-655 sensors. Sensors were calibrated using Coyle-Lucien complex soil taken from a location near the tallgrass prairie site in 2013. The calibration equation used was

$$\theta = 0.107\sqrt{K_a} - 0.119\sqrt{EC} - 0.105 \tag{1}$$

where θ is the volumetric soil water content [m³ m³]. Using the volumetric water content values resulting from Equation 1, we calculated depth-weighted mean (i.e., mean of three sensor profiles) daily root zone volumetric soil moisture values for all available dates for each site. Depth-weighted root zone soil moisture values at these sites and at Oklahoma Mesonet stations were calculated by assuming soil moisture sensors were located at the center of a given soil layer (i.e., the data recorded by the sensor at 5 cm is representative of the condition of the layer from 0-10 cm, etc.), with the exception of the tallgrass prairie site, where soil moisture sensor depths necessitated the use of a trapezoidal integration function for depth weighting. Due to datalogger storage limitations and remote site connectivity problems, portions (ranging from 14.2–33.8%) of measured data are missing after the installation date at each site. Station installation dates are shown in Table 1.

2.2. Soil water balance model

The dual crop coefficient form of the FAO-56 method is a well-known empirical method used to estimate soil evaporation and crop transpiration (together, ET_c) using meteorological data and tabular crop coefficients (Allen et al., 1998). Inputs for the model include: daily estimates of reference evapotranspiration (ET_o), which are calculated from measured wind speed, air temperature, rainfall, incoming solar radiation, and relative humidity data; daily basal crop coefficient (K_{cb}) values which approximate the ratio of transpiration that would occur in the absence of water stress to reference evapotranspiration; daily plant height and rooting depth estimates; soil properties for the surface layer and the full root zone including sand and clay percentages, soil volumetric water content at field capacity, and soil volumetric water content at wilting point; the fraction of soil covered by plant residue; and the soil volumetric moisture content at the beginning of the simulation.

Daily ET_o values for a short crop reference surface are calculated using the Penman-Monteith method as described in the FAO-56 procedure. A water stress coefficient (K_s), which reduces vegetation transpiration when the amount of available soil water in the root zone drops below a defined threshold, and a soil evaporation coefficient (K_e), which reduces soil evaporation when the water content of the surface soil decreases, are calculated daily based on the estimated available soil water storage. Along with the K_{cb} values, the estimated K_s and K_e values are used to scale ET_o according to

$$ET_{c_adj} = (K_s \times K_{cb} + K_e) ET_0$$
 (2)

where ET_{c_adj} is the crop evapotranspiration, adjusted for soil water stress conditions (Allen et al., 1998).

ET_{c adj} values are calculated as part of the daily water balance:

$$D_{ri} = D_{ri-1} - (P - RO) + ET_{c_{adi}} + DP$$
 (3)

where D_{ri} is the current root zone depletion (i.e., deficit relative to field capacity), $D_{ri\cdot 1}$ is root zone depletion from the previous day, P is precipitation, RO is surface runoff, and DP is deep percolation (Allen et al., 1998). Deep percolation is non-zero only on days when the soil water content exceeds field capacity and is estimated by

Table 2 Surface and full profile mean depth-weighted sand and clay contents, porosity, soil volumetric water contents at field capacity (θ_{-10}) and wilting point (θ_{-1500}), and the depth of soil subject to evaporation (Z_e).

	Surface	Surface				Full profile					_
Site	Sand %	Clay %	Porosity m ³ m ⁻³	$^{\theta_{-10}}_{m^3m^{-3}}$	$\theta_{-1500} \\ m^3 m^{-3}$	Sand %	Clay %	Porosity m ³ m ⁻³	$^{\theta_{-10}}_{m^3m^{-3}}$	θ ₋₁₅₀₀ m ³ m ⁻³	$Z_{\rm e} \ m$
Loblolly Pine Plantation	44.8	10.4	0.40	0.28	0.03	36.9	20.9	0.38	0.33	0.09	0.13
Mixed hardwood forest	80.3	3.74	0.46	0.09	0.02	86.1	4.23	0.48	0.07	0.02	0.11
Cropland	25.8	19.9	0.46	0.31	0.10	21.3	24.5	0.45	0.32	0.11	0.14
Tallgrass Prairie	35.0	21.2	0.51	0.30	0.13	20.0	40.9	0.44	0.32	0.21	0.13

$$DP = P - RO - ET_{c_{odi}} - D_{ri-1} \tag{4}$$

On days when water drains from the soil profile (i.e., when DP > 0), D_r is equal to zero. Additional calculations within the model include the estimation of the total available soil water (TAW), which is estimated by

$$TAW = (\theta_{-10} - \theta_{-1500}) Z_r$$
 (5)

where Z_r is the rooting depth [mm]. Finally, daily plant available water (PAW) values are estimated as

$$PAW = TAW - D_r (6)$$

Daily PAW estimates were converted to depth-weighted values of root-zone volumetric soil moisture (θ) [m³ m⁻³] according to:

$$\theta = \frac{PAW}{L} + \theta_{-1500_{dw}} \tag{7}$$

where L is the thickness of the soil profile and where $\theta_{-1500dw}$ is the depth-weighted mean value of surface and full profile θ_{-1500} values given in Table 2.

The K_s coefficient in Eq. 2 is calculated within the model according to the following equation:

$$K_s = \frac{TAW - D_r}{(1 - p)TAW}, D_r > pTAW$$
(8)

where p is the depletion fraction, or the average fraction of TAW that can be depleted from the root zone before plant water stress occurs. The K_e coefficient is calculated as:

$$K_e = min(\{K_r(K_{c_max} - K_{cb})\}, \{f_{ew}K_{c_max}\})$$
(9)

where K_r is a dimensionless evaporation reduction coefficient which is dependent upon the cumulative depth of water evaporated from the soil surface layer, $K_{c,max}$ represents an upper limit on evapotranspiration, and f_{ew} is the fraction of soil that is exposed and wetted (i.e., the fraction of soil from which evaporation occurs).

The $K_{C,max}$ parameter is imposed to limit ET based on restraints on available energy, and is typically calculated according to:

$$K_{c.max} = \max\left(\left\{1.2 + \left[0.04(u_2 - 2) - 0.004(RH_{min} - 45)\right]\left(\frac{h}{3}\right)\right\}, \left\{K_{cb} + 0.05\right\}\right)$$
(10)

where u_2 is the mean daily wind speed at 2 m above the ground surface $[m\,s^{-1}]$, RH_{min} is the minimum relative humidity for each day [%], and h is the mean maximum plant height [m]. Equation 10 leads the model to utilize whichever calculated value is greater (i.e., the first or second argument of the max function). Normally, $K_{c,max}$ is no more than ~ 1.3 (Allen et al., 1998). However, in the simulations of the forested sites, Eq. (10) apparently overestimated $K_{c,max}$ due to the larger height (h) of the forest canopy as compared to typical agronomic crops, and the calculated $K_{c,max}$ values were often >1.7. This led to unrealistically high estimates of $ET_{c,adj}$ for the forested sites (annual $ET_{c,adj} >>$ annual P). For this reason, for the forested locations, $K_{c,max}$ was set equal to $K_{cb} + 0.05$ (i.e., the right-hand portion of the function in Eq. 10).

Irrigation inputs were not considered because all of the study

locations are rainfed. Additionally, surface runoff was assumed to be negligible for these nearly-level sites. Based on measured daily precipitation values as well as the hydrologic soil groups and estimated curve numbers of the study locations, surface runoff likely occurred on $<\!5\%$ of simulation days across all sites.

The FAO-56 method was developed for and has been traditionally applied in agricultural cropping systems, but the method has shown the potential to estimate vegetation water use and soil water dynamics under diverse land covers types by using remote sensing vegetation indices data as a proxy for K_{cb} (Sánchez et al., 2010). Here, we applied a vegetation index-based approach at four locations in Oklahoma with diverse land cover types for the period from January 1, 2000 - June 8, 2020. While simulations were run for >20 years to characterize long-term patterns, measured soil moisture data are only available at the four study sites in recent years (see Table 1). For this reason, we focus our analysis and discussion on the period for which measured soil moisture data are available at each site. Normalized difference vegetation index (NDVI) and enhanced vegetation index (EVI) data from the MODIS instruments aboard NASA's Aqua and Terra satellites were tested in order to determine which VI product yielded crop coefficients that resulted in the most accurate estimations of volumetric soil water content at the four study sites (see Appendix A). The best-performing VI dataset and meteorological data from the Oklahoma Mesonet were used as the primary model inputs (Fig. 1) (Huete et al., 1999; McPherson et al., 2007).

2.3. Geographical and meteorological inputs

Geographical inputs necessary for the model include elevation and longitude and latitude, which are used to adjust the psychrometric constant to account for changes in atmospheric pressure with altitude and to account for variations in extraterrestrial radiation by latitude. Precipitation records for each monitoring station are also required, as are daily estimates of reference evapotranspiration (ET₀). Estimates of ET₀ were produced using daily data from the Oklahoma Mesonet station nearest to each independent soil moisture monitoring location. Any missing meteorological records were filled using data from the next nearest Oklahoma Mesonet station (McPherson et al., 2007). If no data were available from the next nearest station, the remaining missing records were filled in using linear interpolation. The distance between the Mesonet stations and the monitoring locations ranged from 0.13 km to 23.1 km (Fig. 1, Table 1).

The effects of non-reference (i.e., non-irrigated) ground cover on ET_0 estimates were accounted for using daily dew point temperature and relative humidity data according to the method described by Allen (1996). Dew point temperatures were calculated from daily temperature and relative humidity data as follows:

$$e_{sat} = 6.1365e^{\left(\frac{17.502T_{\min}}{240.97+T_{\min}}\right)}$$
 (11)

$$e = \left(\frac{RH}{100}\right)e_{sat} \tag{12}$$

$$T_{dew} = 240.97 \times \frac{\ln\left(\frac{\epsilon}{6.1365}\right)}{17.502 - \ln\left(\frac{\epsilon}{6.1365}\right)}$$
 (13)

where e_{sat} is the saturation vapor pressure [mb] at the minimum daily temperature, e is the actual vapor pressure [mb], T_{min} is the minimum daily temperature [°C], and RH is the relative humidity (Buck, 1981; Allen et al., 1998). This correction was made for days when the minimum observed air temperature was >2°C above the calculated dew point temperature, and the resulting dew point temperatures and relative humidity data were used to calculate adjusted daily maximum and minimum temperature values for use in the ET₀ calculations according to the procedure described by Allen (1996). These corrections were necessary on 27% of days across all sites and resulted in a 2.7% decrease in ET₀, on average.

In addition to corrections for non-reference ground cover, precipitation record inputs at the forested sites were adjusted to account for canopy and understory interception, assuming 2 mm of interception lost at the onset of every precipitation event. This interception value is similar to that found by Zou et al. (2015), who reported canopy storage capacity (i.e., interception rates) of 2.14-3.44 mm in eastern redcedar (Juniperus virginiana) woodlands. This adjustment was necessary because all precipitation data were collected at the nearest Mesonet station (i.e., outside the forested area) and are not necessarily representative of the precipitation experienced at the soil surface under the forest canopy and residue. This adjustment led to a decrease in effective annual precipitation of \sim 141 mm yr $^{-1}$ at the mixed hardwood forest site and \sim 157 mm yr⁻¹ at the pine plantation site. While there may also be significant interception at the tallgrass prairie location during certain times of the year (Zou et al., 2015), due to the dynamic nature of the above ground vegetation, those effects were not considered here.

2.4. Remote sensing inputs

MODIS NDVI and EVI composite imagery at a 250-m resolution and 16-day return period were used here (MOD13Q1 and MYD13Q1 products). Because these images are available from either the Aqua or Terra satellite at 16-day intervals and because the satellites' return intervals are offset from one another by 8 days, a complete image is available every 8 days. EVI and NDVI are calculated as (Huete et al., 2008):

$$EVI = G\left(\frac{\rho_{NIR} - \rho_{red}}{\rho_{NIR} + C_1 * \rho_{red} - C_2 * \rho_{blue} + L}\right)$$
(14)

$$NDVI = \frac{(\rho_{NIR} - \rho_{red})}{(\rho_{NIR} + \rho_{red})}$$
 (15)

where ρ are corrected or partially atmosphere-corrected surface reflectances of the near infrared $(\rho_{NIR}),$ red $(\rho_{red}),$ and blue (ρ_{blue}) bands, L is the canopy background adjustment that addresses NIR and red radiant transfer through a canopy, and $C_1,\,C_2$ are the coefficients of the aerosol resistance term, which uses the blue band to correct for aerosol influences in the red band (Huete et al., 2002). The coefficients adopted in the EVI algorithm are, $L=1,\,C_1=6,\,C_2=7.5,$ and G (gain factor) = 2.5 (Huete et al., 1994; Huete et al., 1997).

All remote sensing data were downloaded using a custom script in the JavaScript API within the Google Earth Engine Code Editor (Gorelick et al., 2017). This script defined a bounding rectangle around each monitoring station which contained only the dominant land cover type based on Google Earth aerial imagery. Area-weighted mean VI values for each area were calculated for each 16-day composite image, and a time series of VI values for each location was saved in a text file. After download, VI data were processed using a custom MATLAB script.

There is some evidence that EVI may be more suitable than NDVI for the current application for a number of reasons, including that EVI images are less likely to saturate when considering dense canopies due to the addition of the blue reflectance band (Gao et al., 2000). Additionally, EVI is designed to separate the background signal of the soil from that of the plant canopy, EVI is more responsive than NDVI to vegetation structural variations, and EVI data have been shown to be more highly correlated with ET than NDVI data (Gao et al., 2000; Wang et al., 2007).

Six different approaches for estimating K_{cb} values from NDVI and EVI data were tested. This included using generalized equations and site-specific equations from the literature (see Appendix A for description of each method and testing results). K_{cb} values from each estimation method were used within the FAO-56 model in order to determine which method yielded the most accurate estimations of soil moisture as compared to measured data at the four focus sites. While all of the K_{cb} estimation methods performed similarly, the method with the lowest mean error was found to be:

$$K_{cb} = \frac{EVI - EVI_{min}}{EVI_{max} - EVI_{min}}$$
 (16)

with a mean r value of 0.68, mean MAE of 0.04 m³ m⁻³, and mean MBE of 0.002 m³ m⁻³ across sites (Table A1). This generalized equation follows the method described by Choudhury et al. (1994) and Glenn et al. (2010), where EVI is the mean observed EVI value of the defined area for each image, EVI_{min} is the minimum EVI value for a given site during the study period, and EVI_{max} is the maximum EVI value for a given site during the study period. Because it performed slightly better than the other K_{cb} estimation equations, does not rely upon a site-specific calibration, and because of the greater suitability of the EVI product over NDVI for the present study, Eq. 13 alone was used for the remainder of analyses. Following the calculation of K_{cb} values at 8-day intervals, values were interpolated linearly between image dates to produce daily K_{cb} values for the simulation period similar to the method used by Sánchez et al. (2010) and Sánchez et al. (2012a).

2.5. Vegetation characteristic inputs

In addition to the data described above, the model requires daily estimates of vegetation height and rooting depth. Vegetation heights for the mixed hardwood forest site were assumed to be static and to be equal to 10.0 m, which lies within the range of tree heights in the cross timbers of Oklahoma reported by Oklahoma Forestry Services (2010). A mean tree height of 9.4 m was reported for the pine plantation location used in this study by Dipesh et al. (2014) and was used here, also assuming a static vegetation height. Dynamic daily vegetation heights for the cropland site were estimated by multiplying daily Kcb values by 2.0 m, the vegetation height for field corn reported by Allen et al. (1998), which was grown at the site during the validation period. This method allowed the vegetation height to vary according to vegetation greenness rather than according to a defined growth curve, which was necessary due to the varying crop rotations implemented at the site and due to the lack of crop type data in many years. The same method was used at the tallgrass prairie site, using a maximum plant height of 1.0 m based on observations at the field site.

Rooting depths for the two forested locations and for the cropland site were set equal to 1.2 m to match the effective soil depth to which soil moisture content was measured by the installed sensors. The active rooting depth may be \geq 1.2 m for these locations, as tree roots were observed down to at least 1.0 m depth at the forested sites during sensor installation and crops grown at the cropland site can have effective rooting depths of 1.0-2.0 m (Allen et al., 1998). The rooting depth used for the tallgrass prairie site was set to 0.65 m to match the shallower soil moisture measurement depths at that location. The true rooting depth at

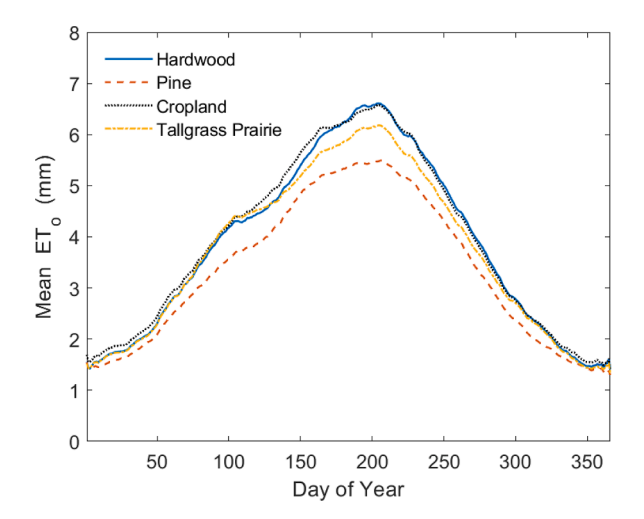


Fig. 3. Daily mean reference evapotranspiration (ET_0) from January 1, 2000 – June 8, 2020 for each study site, smoothed using a 30-day centered moving average.

the tallgrass prairie site is likely limited by the soil depth, which is <0.3 m in some places and commonly <1.0 m.

2.6. Soil property inputs

Information regarding the soil properties of the modeled area is also required, including the depth of soil from which evaporation may occur (Z_e), θ_{-10} and θ_{-1500} at the surface and for the full soil profile, and soil volumetric water content on the first date of simulation. Z_e was calculated for each location based on the sand content of the surface soil as described in Allen et al. (1998) (Table 2). The necessary soil properties

were estimated from soil cores taken at each monitoring site, and mean soil properties of the uppermost soil samples (5-cm depth) were used to represent the soil surface properties in the model.

Mean depth-weighted soil properties (i.e., mean values of the triplicate profiles' soil properties) were used to represent the soil physical properties of the full soil profile at each site within the model (Table 2). At the mixed hardwood forest, loblolly pine plantation, and cropland sites these depth-weighted properties were calculated by assuming that each soil moisture sensor was located at the center of a given soil layer (i. e., the data recorded by the sensor at 5 cm is representative of the condition of the layer from 0-10 cm, etc.). At the tallgrass prairie site, due to the sensor installation depths, a trapezoidal integration was used to estimate profile soil properties to a depth of 65 cm. Soil moisture values on the first day of the simulation were assumed to be the same as those at the nearest Oklahoma Mesonet station, or to be halfway between the depth-weighted $\theta_{\cdot 10}$ and $\theta_{\cdot 1500}$ values if no Mesonet data were available.

2.7. SMAP root zone soil moisture data

NASA-USDA SMAP root zone soil moisture data were compared with model-estimated soil moisture values at each site. These soil moisture data are available every three days at a spatial resolution of 10 km. The data represent conditions to a depth of 1.0 m and are developed by integrating radiometer-derived Soil Moisture Active Passive (SMAP) Level 3 soil moisture observations into the modified two-layer Palmer model using a 1-dimensional Ensemble Kalman Filter data assimilation approach (Entekhabi et al., 2010; (Sazib et al., 2018)). Like VI data, data were processes in Google Earth Engine, which was used to produce area-weighted mean SMAP soil moisture values for each study site.

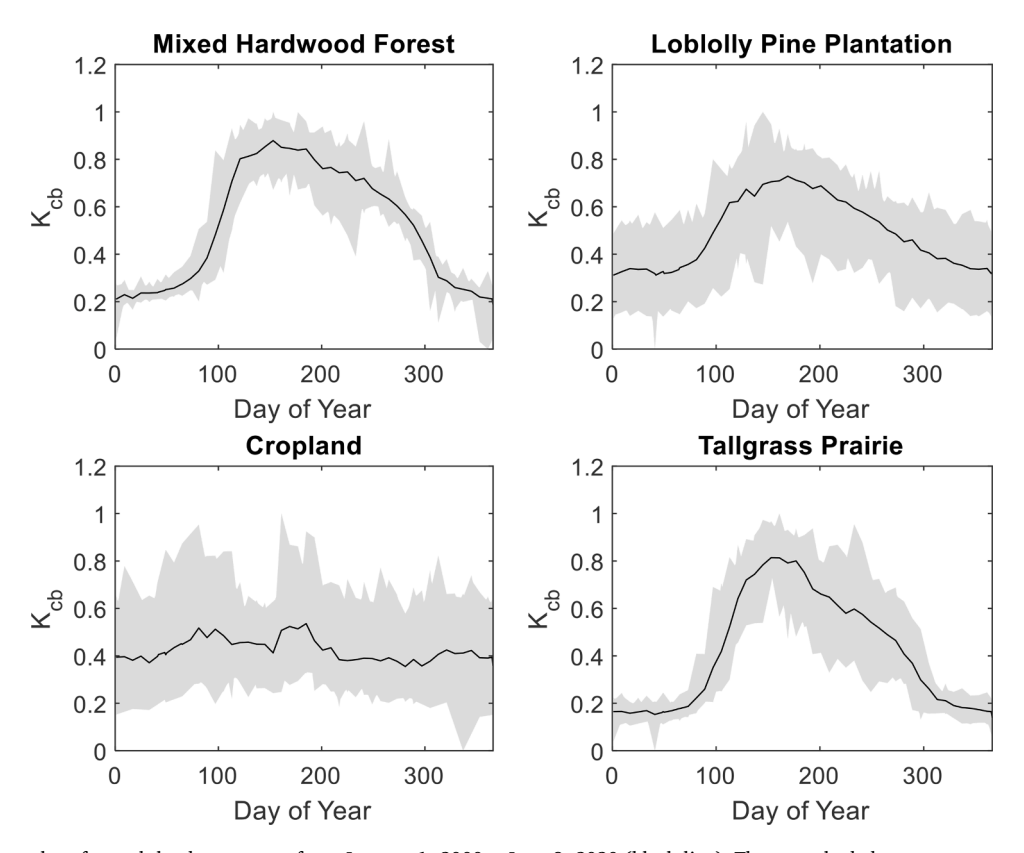


Fig. 4. Mean daily K_{cb} values for each land cover type from January 1, 2000 – June 8, 2020 (black line). The gray shaded areas represent the full range of daily K_{cb} values.

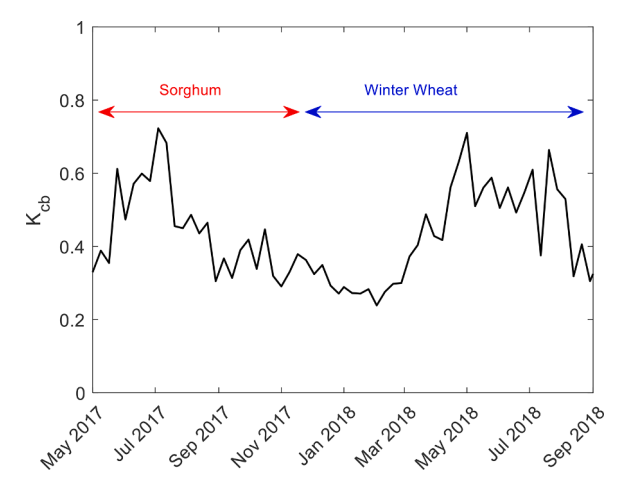


Fig. 5. Examples of growing season K_{cb} curves for the cropland site when planted with a warm season crop (sorghum) followed by a cool season crop (winter wheat).

3. Results and discussion

3.1. ETo estimates

Mean annual ET $_{\rm o}$ values at each location for the full simulation period range from 1219 mm yr $^{-1}$ in the loblolly pine plantation to 1425 mm yr $^{-1}$ at the cropland site, with intermediate values of 1352 mm yr $^{-1}$ at the tallgrass prairie and 1403 mm yr $^{-1}$ at the mixed hardwood forest site. Daily ET $_{\rm o}$ estimates ranged from 0.24 to 12.0 mm d $^{-1}$ at the mixed hardwood forest location, from 0.32 to 9.55 mm d $^{-1}$ at the loblolly pine plantation location, from 0.30 to 12.3 mm d $^{-1}$ at the cropland location, and from 0.26 to 10.8 mm d $^{-1}$ at the tallgrass prairie location. Smoothed mean daily ET $_{\rm o}$ values for each day of the year during the study period are shown in Fig. 3. Mean daily ET $_{\rm o}$ peaked on the 192 $^{\rm nd}$ day of the year (July 10 or 11) in the loblolly pine plantation and peaked slightly later

Oct 2018 Jan 2019 Apr 2019 Jul 2019 Oct 2019 Jan 2020 Apr 2020

on the $201^{\rm st}$ day of the year (July 19 or 20) at the mixed hardwood forest, tallgrass prairie, and cropland sites.

Annual ET $_0$ values found for the study sites are similar to long-term (2005-2019) average ET $_0$ values reported by the nearest Oklahoma Mesonet stations (Sutherland et al., 2005; Oklahoma Mesonet webpage). The mean annual ET $_0$ value of 1219 mm yr $^{-1}$ found at the loblolly pine plantation is comparable to the value of 1204 mm yr $^{-1}$ reported for the nearby Idabel Mesonet site. The ET $_0$ values of 1352 mm yr $^{-1}$ estimated for the tallgrass prairie site and 1403 mm yr $^{-1}$ for the hardwood forest site are comparable to the value of 1367 reported for the Marena Mesonet station nearby both sites. The mean annual ET $_0$ value of 1425 mm yr $^{-1}$ estimated for the cropland is close to the reported value of 1427 mm yr $^{-1}$ at the nearby Chickasha Mesonet site. Distances from the study sites to the Mesonet sites mentioned here are given in Table 1, with the exception of the Mesonet site nearest the hardwood forest site, where

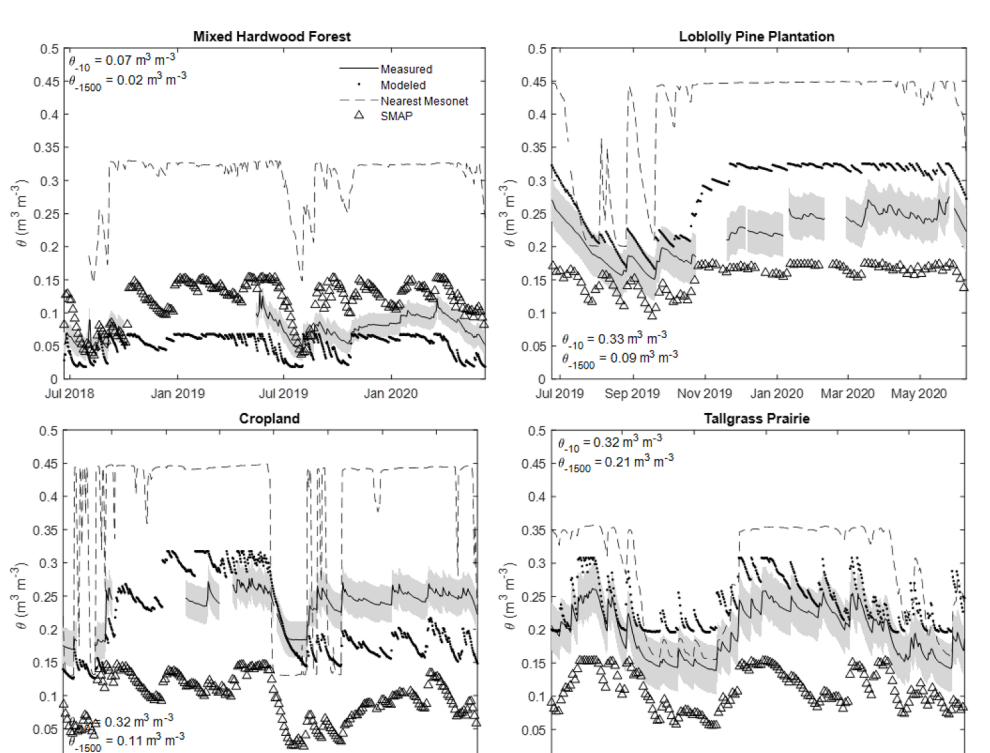


Fig. 6. Mean (solid line) and standard deviation (shaded area) of measured root-zone soil volumetric water content under each land cover type, modeled root-zone soil volumetric water content (black dots), measured root-zone soil volumetric water content from the nearest Oklahoma Mesonet station (dashed line), and NASA-USDA SMAP root zone soil moisture data at each site (triangles). All data have been depth-weighted according to the procedure described in section 2.1. Measured root-zone soil volumetric water contents at field capacity (θ_{-10}) and permanent wilting point (θ_{-1500}) are also given for each site. Select dates are shown for the tallgrass prairie site to preserve figure legibility.

Oct 2015

Jan 2016

Apr 2016

Jul 2015

Table 3
Pearson correlation coefficient (*r*), mean absolute error (MAE), and mean bias error (MBE) calculated by comparing daily volumetric water content estimated by the water balance model and measured volumetric water content each independent monitoring site (modeled v. measured), by comparing independent volumetric water content measured under each land cover type and measured volumetric water content at the Oklahoma Mesonet station nearest the monitoring site (measured v. Mesonet), and by comparing measured volumetric water content each independent monitoring site with SMAP soil moisture (Measured v. SMAP).

	Modeled v. Measured			Measured v. Mesonet			Measured v. SMAP		
Site	r -	$^{\rm MAE}_{\rm m^3~m^{-3}}$	MBE m ³ m ⁻³	r -	$^{\rm MAE}_{\rm m^3~m^{-3}}$	MBE m ³ m ⁻³	r -	$^{\rm MAE}_{\rm m^3~m^{-3}}$	MBE m ³ m ⁻³
Loblolly pine plantation	0.92	0.06	-0.05	0.65	0.18	0.15	0.85	0.07	0.05
Mixed hardwood forest	0.70	0.03	0.02	0.76	0.22	0.14	0.74	0.04	-0.02
Cropland	0.50	0.06	0.02	0.70	0.16	0.10	0.56	0.15	0.11
Tallgrass prairie	0.80	0.04	-0.02	0.75	0.09	0.06	0.83	0.12	0.04
MEAN	0.73	0.05	-0.01	0.72	0.16	0.11	0.75	0.10	0.05

long-term ET_0 data are not available. The Marena Mesonet station is located 17.5 km from the hardwood forest site.

3.2. Kcb curves

Mean daily K_{cb} values during the study period, as well as maximum and minimum Kcb values for each day of the year, are shown in Fig. 4. Kcb values during the study period ranged from 0.0-1.0 for all land cover types (see Eq. 13). The curves of the forested and tallgrass prairie sites show similar patterns, with an exponential increase in Kcb values in the spring, small declines during the summer months, and a sharp decline indicating decreasing plant greenness and plant senescence in the fall and winter months. The mean cropland K_{cb} curve shows little change throughout the calendar year, with small peaks near day 100, day 175, and day 320. The relatively constant cropland mean K_{cb} values and multiple small peaks throughout the year in Fig. 4 are likely due to the production of crops with different peak growth periods (e.g., winter wheat versus sorghum) during different years of the simulation period. An example of different seasonal Kcb curves for cool season (winter wheat) and warm season (sorghum) crops is shown in Fig. 5. This figure shows the different K_{cb} curves for two crop types, with peak K_{cb} values for sorghum occurring in early July and peak Kcb values for winter wheat occurring in late April and early May.

The K_{cb} curves for the study locations are similar to those in prior studies which estimated the basal crop coefficient using VI data. For example, Sánchez et al. (2012a) reported K_{cb} values estimated from VI data ranging from near zero to ~ 0.75 for barley cropland during a single growing season. The same study reported K_{cb} values ranging from zero to ~ 0.50 for grassland, which is slightly lower than the mean peak value of ~ 0.80 found in this study. However, it is important to note that Sánchez et al. (2012a) considered only one growing season, while Fig. 4 considers > 20 years of VI data. Campos et al. (2017) used the soil adjusted vegetation index (SAVI) to estimate K_{cb} for a site under maize and soybean rotation and found that K_{cb} reached a maximum value of 0.95 under maize and 0.90 under soybean. These values are more comparable to the maximum K_{cb} values found for the cropland site (Figs. 4, 5).

The dual crop coefficient method has been most commonly applied to cropland and grassland locations, and to our knowledge, no comparable studies have been carried out in forested ecosystems that would allow for a comparison of K_{cb} curves at the mixed hardwood forest and loblolly pine plantation sites. However, Allen et al. (1998) suggests a year-round K_{cb} value of 1.0 for conifer trees. In contrast, Fig. 4 suggests that even for evergreen species the K_{cb} value is not constant and fluctuates seasonally, which indicates that using a constant K_{cb} value may lead to incorrect estimates of $ET_{c\ adj}$.

3.4. Comparison of modeled and measured soil moisture

Model-estimated root zone volumetric soil moisture for the study ranged from 0.02 to 0.07 $\rm m^3~m^{-3}$ under mixed hardwood forest, from

0.08 to 0.33 m^3 m^{-3} under loblolly pine, from 0.11 to 0.32 m^3 m^{-3} under cropland, and from 0.20 to 0.31 m^3 m^{-3} under tallgrass prairie. Mean daily volumetric soil moisture was greatest year-round at the tallgrass prairie location, which had the finest soil texture among the study sites, and lowest year-round at the hardwood forest site, which had the coarsest soil texture. The extremely low values of soil moisture at the hardwood forest site are likely a result of the high sand content of the soil at the site (>80% sand, Table 2).

Pearson correlation coefficient values across all sites indicate a moderate to high level of agreement between model estimated and measured root zone soil moisture. The model was able to estimate soil moisture dynamics moderately well at all sites, though some overestimations and underestimations are evident at times at each site (Fig. 6). These discrepancies are most likely a result of the values of θ_{-10} and θ_{-1500} measured at the sites. These values are shown in each subfigure of Fig. 6 and represent the effective range of soil moisture values for each site, as the FAO-56 model uses these values as upper and lower limits on soil water storage. The greatest *r* values were found for the loblolly pine plantation site (r = 0.92), and the lowest values were found for the cropland site (r = 0.50) (Table 3). The range of r values from this study is comparable to those found by Schnur et al. (2010), who reported r values from 0.74 to 0.94 when applying a trained linear regression model to estimate 0-50 cm soil moisture values at distant, unmonitored sites using NDVI data. Our findings are also similar to those reported by Owe et al. (1988), who found an r value of 0.82 for their model, which used microwave brightness temperature and NDVI to estimate soil moisture at an unmonitored location.

Model error and bias were low at all sites, with mean absolute error (MAE) ranging from 0.03 to 0.06 m 3 m $^{-3}$ (Table 3). The greatest MAE values were found for the cropland and loblolly pine sites, while the lowest MAE value was found for the mixed hardwood forest site. The level of error found in the present study is greater than that reported by Sánchez et al. (2010), who reported RMSE values ranging from 0.01 to 0.03 m 3 m $^{-3}$, but similar to that reported by Sánchez et al. (2012b), who reported RMSE values ranging from 0.01 to 0.11 m 3 m $^{-3}$. Mean bias error (MBE) ranged from -0.05 to 0.02 m 3 m $^{-3}$, with the greatest absolute MBE observed for the loblolly pine plantation and the lowest absolute MBE found for the mixed hardwood forest site. The level of bias found in the present study is also comparable to that reported by Sánchez et al. (2012b), who reported bias values ranging from 0.00 to 0.04 m 3 m $^{-3}$.

3.5. Comparison of soil moisture measurements from independent monitoring stations and Mesonet

We also compared measured soil moisture under each land cover type to measured soil moisture at the nearest Mesonet station in order to determine differences in soil moisture dynamics and magnitude under different land cover types (Table 3). The greatest r value was found for the tallgrass prairie site (r = 0.77), and the lowest value was found for the loblolly pine plantation (r = 0.65). The moderately low correlation

Table A1Pearson correlation coefficient (*r*), mean absolute error (MAE), and mean bias error (MBE) for six K_{cb} estimation methods.

K _{cb} method	Land cover type	r	MAE	MBE
		-	${ m m}^3{ m m}^{-3}$	${\rm m}^{3}~{\rm m}^{-3}$
K _{cb-EVI1}	Mixed Hardwood Forest	0.70	0.03	0.02
	Loblolly Pine Plantation	0.92	0.06	-0.05
	Cropland	0.50	0.06	0.02
	Tallgrass Prairie	0.80	0.04	-0.02
K _{cb-EVI2}	Mixed Hardwood Forest	0.69	0.03	0.02
	Loblolly Pine Plantation	0.96	0.05	-0.04
	Cropland	0.51	0.06	0.02
	Tallgrass Prairie	0.76	0.03	-0.02
K _{cb-Guerschman}	Mixed Hardwood Forest	0.67	0.03	0.02
	Loblolly Pine Plantation	0.97	0.04	-0.02
	Cropland	0.50	0.06	0.03
	Tallgrass Prairie	0.79	0.04	-0.02
K _{cb-Bausch}	Mixed Hardwood Forest	0.66	0.03	0.02
	Loblolly Pine Plantation	0.96	0.04	-0.01
	Cropland	0.48	0.06	0.03
	Tallgrass Prairie	0.74	0.03	-0.02
$K_{\mathrm{cb-Kamble}}$	Mixed Hardwood Forest	0.69	0.03	0.02
	Loblolly Pine Plantation	0.96	0.04	-0.01
	Cropland	0.49	0.06	0.03
	Tallgrass Prairie	0.77	0.03	-0.02
$K_{cb ext{-}Tasumi}$	Mixed Hardwood Forest	0.66	0.03	0.02
	Loblolly Pine Plantation	0.96	0.04	-0.01
	Cropland	0.47	0.06	0.03
	Tallgrass Prairie	0.74	0.03	-0.02

(r=0.70) between soil moisture at the cropland site and the nearby Oklahoma Mesonet station may be a result of the dichotomous nature of soil moisture dynamics under cool-season crops (such as winter wheat) and warm-season native grasses growing at the Mesonet station (Patrignani and Ochsner, 2018). The soil moisture estimates from the model were more strongly correlated with the measured soil moisture data than were the data from the nearest Mesonet site for the loblolly pine plantation site and the tallgrass prairie site, but not for the other two sites

The error and bias levels were much greater between soil moisture measurements from the nearest Mesonet station and soil moisture at the independent monitoring sites compared to those found between modelestimated soil moisture and independent monitoring sites (Table 3, Measured v. Mesonet). Mean absolute error (MAE) for the nearest Mesonet site ranged from 0.09 to $0.22 \text{ m}^3 \text{ m}^{-3}$, with the greatest MAE at the mixed hardwood forest and lowest MAE at the tallgrass prairie site. Mean bias error ranged from 0.06 to $0.15 \,\mathrm{m}^3 \,\mathrm{m}^{-3}$, with the greatest MBE observed at the loblolly pine plantation and the lowest MBE at the tallgrass prairie. It is likely that these sites exhibited the highest and lowest levels of bias because of their large and small distances between the independent stations and the nearest Mesonet station, respectively (Table 1). While the dynamics of soil moisture between Mesonet and independent monitoring stations are moderately correlated, there are often large errors and biases, which highlights the need for improved estimations of soil moisture under these diverse land cover types. Our findings indicate that soil moisture estimates from the model developed here are better indicators of the soil moisture status across diverse land cover types than are soil moisture measurements from in situ monitoring stations located exclusively under grassland.

3.6. Comparison of modeled and SMAP soil moisture data

Finally, we compared model-estimated soil moisture data to NASA-USDA SMAP root zone soil moisture data at each site (Table 3). Our results indicate that while SMAP data capture soil moisture dynamics slightly better than the model at several sites, model-estimated soil moisture has lower MAE and MBE values on average across sites than SMAP data. This finding suggests that the method used here, if adapted to estimate soil moisture over large areas using 250×250 m resolution

VI data, may be capable of accurately estimating full root zone soil moisture under a wide variety of land cover types at a much higher spatial resolution than most currently operational remote sensing soil moisture products.

4. Conclusions and future work

Soil moisture estimates developed using site-specific VI data and a simple water balance approach were generally correlated with independently measured soil moisture values for the root zone under diverse land cover types. Further, model-estimated soil moisture values were closer to the measured values under each land cover type than were soil moisture measurements under grassland at the nearest Oklahoma Mesonet station. This is particularly of note because the water balance model applied here was developed specifically for agricultural cropping systems, but our results indicate that, with further improvements, the model can produce useful estimates of soil moisture when applied in other, non-agricultural vegetation types.

The results shown here represent a valuable contribution to the field in that 1) our findings demonstrate that soil moisture under diverse vegetation types is substantially different from that at nearby grassland monitoring sites; 2) despite over- and under-estimating soil moisture during certain times, our model-estimated soil moisture values have a high level of accuracy and low bias across land cover types, as indicated by the results shown in Table 3; 3) model-estimated soil moisture values represent root zone conditions and thus may be more useful for some purposes than remote sensing soil moisture data, which typically represent conditions in the top 5 cm of soil; 4) the method incorporates site-specific VI data rather than generic tabular data, which allows the FAO-56 model to be applied to produce estimates of soil moisture under non-agricultural land cover types that were not considered in the original model; and 5) unlike most prior studies, the Kcb estimation method used here relies upon widely-available historical VI data rather than a site-specific calibration, making this method widely and easily applicable.

Further, while the Oklahoma Mesonet is one of the foremost soil moisture monitoring networks in the world and provides data essential for many applications, the large discrepancies between soil moisture values measured at the Mesonet stations and in adjacent, contrasting land cover types indicates that ignoring heterogeneity in soil moisture across land cover types is likely to lead to significant errors when applying these data. Future work should aim to refine the approach developed here and to create a distributed model that applies the method over larger areas (i.e., state or regional scale).

Declaration of Competing Interest

The authors declare that they have no known competing financial interests or personal relationships that could have appeared to influence the work reported in this paper.

Acknowledgements

Financial support for this work was provided by the USGS 104(b) program and the Oklahoma Water Resources Center Berry Fellows Program. This research was supported in part by the USDA National Institute of Food and Agriculture through Hatch Project OKL02918 and by the Division of Agricultural Sciences and Natural Resources at Oklahoma State University. Oklahoma Mesonet data are provided courtesy of the Oklahoma Mesonet, which is jointly operated by Oklahoma State University and the University of Oklahoma. Continued funding for maintenance of the network is provided by the taxpayers of Oklahoma. We thank our colleagues from the Oklahoma Mesonet who continually provide research quality data.

Appendix A. Kcb estimation

Raw EVI and NDVI data were converted to Kcb values using six different methods. Three EVI-based equations were tested:

$$K_{cb-EVI_1} = \frac{EVI - EVI_{min}}{EVI_{max} - EVI_{min}}$$
(A.1)

which follows the method described by Choudhury et al. (1994) and Glenn et al. (2010), where EVI is the mean observed EVI value of the defined area for each image, EVI_{min} is the minimum EVI for a given location during the study period, and EVI_{max} is the maximum EVI value for a given location during the study period. The second EVI-based equation was

$$K_{cb-EVI_2} = \frac{EVI}{EVI_{max} - EVI_{min}} \tag{A.2}$$

which is similar to the previous equation, except that it allows for K_{cb} values greater than one, which is often observed in the FAO-56 methodology. A third EVI-based equation from Guerschman et al (2009) was also tested:

$$K_{cb-Guerschman} = K_{cb-max} \left(1 - \exp(-a \times EV_r^{\alpha}) \right)$$
 (A.3)

where $\alpha = 2.38$ and a = 10.22. This equation and the parameter values used are the result of a model calibration across seven sites in Australia with a variety of land cover types, similar to the present study.

In addition to the equations above, three NDVI-based equations were tested in order to determine which vegetation index is most useful for developing the basal crop coefficient. The three NDVI-based equations are:

$$K_{cb-Bausch} = 1.36NDVI - 0.03$$
 (A.4)

from Bausch and Neale (1987), who developed the equation for a corn site in in Colorado,

$$K_{cb-Kamble} = (1.4571 \times NDVI) - 0.1725$$
 (A.5)

from Kamble et al. (2013), who developed the equation using data from a variety of crop types and locations. The final NDVI-based equation is

$$K_{cb-Tasumi} = (1.18 \times NDVI) + 0.04 \tag{A.6}$$

from Tasumi et al. (2006), who developed the equation for an area of mixed vegetation in New Mexico.

Each set of K_{cb} values was tested within the FAO-56 model in order to determine which K_{cb} estimation method yielded the most accurate estimates of volumetric soil moisture as compared to soil moisture data measured at each monitoring site based on the Pearson correlation coefficient (r), mean absolute error (MAE), and mean bias error (MBE) (Table A1).

Appendix B. ET_{c adj} model outputs

Mean estimated annual ET_{c_adj} ranged from 803 mm yr $^{-1}$ in the hardwood forest to 839 mm yr $^{-1}$ in the loblolly pine plantation, with intermediate values of 799 mm yr $^{-1}$ at the cropland site and 752 mm yr $^{-1}$ at the tallgrass prairie. Annual ET_{c_adj} values ranged from 517 to 859 mm yr $^{-1}$ for the mixed hardwood forest site; from 399 to 966 mm yr $^{-1}$ for the loblolly pine plantation site; from 436 to 1028 mm yr $^{-1}$ for the cropland site; and from 315 to 935 mm yr $^{-1}$ for the tallgrass prairie site. The greatest mean annual ET_{c_adj} was found for the loblolly pine plantation, which is likely due to the high annual precipitation rate and therefore higher water availability at this location (Table 1). The lowest ET_{c_adj} values were found at the tallgrass prairie location, which may be because the specified rooting depth for the tallgrass prairie site was the shallowest among all the study locations.

Current estimates of $ET_{c,adj}$ compare relatively well with prior estimates of evapotranspiration (ET) in similar vegetation types. Prior work has estimated annual ET in Oklahoma grasslands ranging from to 640-810 mm yr⁻¹ (Burba and Verma, 2005; Yimam et al., 2014). The current mean annual $ET_{c,adj}$ values for the tallgrass prairie site (752 mm yr⁻¹) fall within the range of these prior estimates. Additionally, this mean $ET_{c,adj}$ value of 752 mm yr⁻¹ is very similar to that reported by Sun et al. (2018), who measured a single-year ET value of 728 mm using an eddy covariance system

installed nearby the independent tallgrass prairie monitoring site.

Wagle et al. (2019) reported seasonal ET values ranging from 652-734 mm and a single-year total ET value of \sim 900 mm for a non-irrigated alfalfa field in central Oklahoma. These values are comparable to the mean annual ET_{c,adj} value of 799 mm yr⁻¹ found at the cropland site. Additionally, similar ET rates were found under agricultural land in central Oklahoma by Liu et al. (2010), who reported an annual value of 778 mm yr⁻¹; by Burba and Verma (2005), who measured ET in winter wheat in north-central Oklahoma using an eddy covariance system and found annual values ranging from 710 mm to 750 mm; and by Yimam et al (2017), whose watershed-scale modeling study in north-central Oklahoma reported an estimated cropland ET value of 713 mm yr⁻¹.

Liu et al. (2010) reported an annual ET value of 854 mm in forest systems in north-central Oklahoma, which is very comparable to the mean annual estimated $ET_{c,adj}$ at the lobbolly pine site (839 mm yr⁻¹) and slightly higher than mean annual estimated $ET_{c,adj}$ at the mixed hardwood forest (803 mm yr⁻¹). Doughty et al. (2016) reported ET values estimated from MODIS satellite data of 650 to >900 mm yr⁻¹ in evergreen forest in southeast Oklahoma, which is comparable to the mean annual $ET_{c,adj}$ value estimated here for the pine plantation. Hennessey et al. (2004) reported ET values of ~600-800 mm yr⁻¹ in a lobbolly pine plantation in southeastern Oklahoma, values which are slightly lower than those found in the present study.

References

- Allen, R.G., 1996. Assessing integrity of weather data for reference evapotranspiration estimation. J. Irrig. Drainage Eng. Am. Soc. Civ. Eng. 112 (2), 97–106.
- Allen, R. G., et al. 1998. Crop evapotranspiration- Guidelines for computing crop water requirements-FAO Irrigation and drainage paper 56. FAO, Rome 300(9): D05109.
- Bausch, W.C., Neale, C.M., 1987. Crop coefficients derived from reflected canopy radiation: a concept. Trans. ASAE 30 (3), 703–709.
- Buck, Arden L., 1981. New equations for computing vapor pressure and enhancement factor. J. Appl. Meteorol. 20 (12), 1527–1532.
- Burba, G.G., Verma, S.B., 2005. Seasonal and interannual variability in evapotranspiration of native tallgrass prairie and cultivated wheat ecosystems. Agric. Forest Meteorol. 135 (1), 190–201.
- Campos, I., Neale, C.M.U., Suyker, A.E., Arkebauer, T.J., Gonçalves, I.Z., 2017. Reflectance-based crop coefficients REDUX: For operational evapotranspiration estimates in the age of high producing hybrid varieties. Agric. Water Manag. 187, 140–153.
- Choudhury, B.J., Ahmed, N.U., Idso, S.B., Reginato, R.J., Daughtry, C.S.T., 1994. Relations between evaporation coefficients and vegetation indices studied by model simulations. Remote Sens. Environ. 50 (1), 1–17.
- Dipesh, K.C., Will, R.E., Lynch, T.B., Heinemann, R., Holeman, R., 2014. Comparison of loblolly, shortleaf, and pitch X loblolly pine plantations growing in Oklahoma. Forest Ecol. 61 (3): 540–547.
- Doughty, R.X.Xiao, Qin, Y., Zhang, Y., 2016. In: Responses of evapotranspiration and gross primary production of forests and grasslands to drought in the Kiamichi watershed of southeast Oklahoma. Oklahoma Governor's Water Conference. htt p://www.eomf.ou.edu/media/gisday/posters/Doughty-Kiamichi-Drought-Resilie ncyXiaoRuss.pdf. Accessed 21 November 2019.
- Entekhabi, D., Njoku, E.G., Neill, P.E.O., Kellogg, K.H., Crow, W.T., Edelstein, W.N., Entin, J.K., Goodman, S.D., Jackson, T.J., Johnson, J., 2010. The soil moisture active passive (SMAP) mission. Proc. IEEE 98 (5), 704–716.
- Ford, T.W., Quiring, S.M., 2013. Influence of MODIS-derived dynamic vegetation on VIC-Simulated Soil Moisture in Oklahoma. J. Hydrometeorol. 14 (6), 1910–1921.
- Gao, X., Huete, A.R., Ni, W., Miura, T., 2000. Optical-biophysical relationships of vegetation spectra without background contamination. Remote Sens. Environ. 74 (3), 609–620.
- Glenn, E.P., Huete, A.R., Nagler, P.L., Hirschboeck, K.K., Brown, P., 2007. Integrating remote sensing and ground methods to estimate evapotranspiration. Crit. Rev. Plant Sci. 26 (3), 139–168.
- Glenn, E.P., Nagler, P.L., Huete, A.R., 2010. Vegetation index methods for estimating evapotranspiration by remote sensing. Surv. Geophys. 31 (6), 531–555.
- Glenn, E.P., Neale, C.M.U., Hunsaker, D.J., Nagler, P.L., 2011. Vegetation index-based crop coefficients to estimate evapotranspiration by remote sensing in agricultural and natural ecosystems. Hydrol. Process. 25 (26), 4050–4062.
- Gonzalez-Dugo, M., Neale, C.M.U., Mateos, L., Kustas, W.P., Prueger, J.H., Anderson, M. C., Li, F., 2009. A comparison of operational remote sensing-based models for estimating crop evapotranspiration. Agric. Forest Meteorol. 149 (11), 1843–1853.
- Gorelick, N., Hancher, M., Dixon, M., Ilyushchenko, S., Thau, D., Moore, R., 2017. Google Earth Engine: Planetary-scale geospatial analysis for everyone. Remote Sens.
- Harpold, A.A., Sutcliffe, K., Clayton, J., Goodbody, A., Vazquez, S., 2017. Does including soil moisture observations improve operational streamflow forecasts in snowdominated watersheds? JAWRA J. Am. Water Resour. Assoc. 53 (1), 179–196.
- Hendrickx, J.M.H., Allen, R.G., Brower, A., Byrd, A.R., Hong, S., Ogden, F.L., Pradhan, N. R., Robison, C.W., Toll, D., Trezza, R., Umstot, T.G., Wilson, J.L., 2016.
 Benchmarking optical/thermal satellite imagery for estimating evapotranspiration and soil moisture in decision support tools. JAWRA J. Am. Water Resour. Assoc. 52 (1), 89–119.
- Hennessey, T.C., Dougherty, P.M., Lynch, T.B., Wittwer, R.F., Lorenzi, E.M., 2004. Long-term growth and ecophysiological responses of a southeastern Oklahoma loblolly pine plantation to early rotation thinning. Forest Ecol. Manag. 192 (1), 97–116.
- Huete, A.R., Liu, H.Q., Batchily, K., van Leeuwen, W.J.D., 1997. A comparison of vegetation indices over a global set of TM images for EOS-MODIS. Remote Sens Environ. 59, 440–451.
- Huete, A., Justice, C., Van Leeuwen, W., 1999. MODIS vegetation index (MOD13). Algorithm Theor. Basis Document 3, 213.

- Huete, A., Justice, C., Liu, H., 1994. Development of vegetation and soil indices for MODIS-EOS. Remote Sens. Environ. 49, 224–234.
- Huete, A., Didan, K., Miura, T., Rodriguez, E.P., Gao, X., Ferreira, L.G., 2002. Overview of the radiometric and biophysical performance of the MODIS vegetation indices. Remote Sens. Environ. 83 (1-2), 195–213.
- Huete, A.; Didan, K., van Leeuwen, W., Miura, T.; Glenn, E. 2008. MODIS vegetation indices. In Land Remote Sensing and Global Environmental Change: NASA's Earth Observing System and the Science of ASTER and MODIS.
- Kerr, Y.H., Waldteufel, P., Wigneron, J.P., Martinuzzi, J.M., Font, J., Berger, M., 2001. Soil moisture retrieval from space: The Soil Moisture and Ocean Salinity (SMOS) mission. Geoscience and Remote Sensing. IEEE Trans. 39 (8), 1729–1735.
- Kumar, S.V., Peters-Lidard, C.D., Tian, Y., Houser, P.R., Geiger, J., Olden, S., Lighty, L., Eastman, J.L., Doty, B., Dirmeyer, P., Adams, J., Mitchell, K., Wood, E.F., Sheffield, J., 2006. Land information system: An interoperable framework for high resolution land surface modeling. Environ. Modell. Softw. 21 (10), 1402–1415.
- Liu, Wenjuan, Hong, Y., Khan, S.I., Huang, M., Vieux, B., Caliskan, S., Grout, T., 2010. Actual evapotranspiration estimation for different land use and land cover in urban regions using Landsat 5 data. J. Appl. Remote Sens. 4 (1), 1–15.
- Lollato, R.P., Patrignani, A., Ochsner, T.E., Edwards, J.T., 2016. Prediction of plant available water at sowing for winter wheat in the Southern Great Plains. Agronomy J. 108 (2), 745–757.
- Lollato, R.P., Ochsner, T.E., Arnall, D.B., Griffin, T.W., Edwards, J.T., 2018. From field experiments to regional forecasts: upscaling wheat grain and forage yield response to acidic soils. Agronomy J. 111 (1), 287–302.
- McPherson, R.A., Fiebrich, C.A., Crawford, K.C., Kilby, J.R., Grimsley, D.L., Martinez, J. E., Basara, J.B., Illston, B.G., Morris, D.A., Kloesel, K.A., 2007. Statewide monitoring of the mesoscale environment: A technical update on the Oklahoma Mesonet. J. Atmos. Oceanic Technology 24 (3), 301–321.
- Mitchell, K.E., Lohmann, D., Houser, P.R., Wood, E.F., Schaake, J.C., Robock, A., Cosgrove, B.A., Sheffield, J., Duan, Q., Luo, L., Higgins, R.W., Pinker, R.T., Tarpley, J.D., Lettenmaier, D.P., Marshall, C.H., Entin, J.K., Pan, M., Shi, W., Koren, V., Meng, J., Ramsay, B.H., Bailey, A.A., 2004. The multi-institution North American Land Data Assimilation System (NLDAS): Utilizing multiple GCIP products and partners in a continental distributed hydrological modeling system. J. Geophys. Res. Atmos. 109 (D7).
- Mohanty, B.P., Cosh, M.H., Lakshmi, V., Montzka, C., 2017. Soil moisture remote sensing: state-of-the-science. Vadose Zone J. 16 (1).
- Ochsner, T.E., Cosh, M.H., Cuenca, R.H., Dorigo, W.A., Draper, C.S., Hagimoto, Y., Kerr, Y.H., Njoku, E.G., Small, E.E., Zreda, M., 2013. State of the art in large-scale soil moisture monitoring. Soil Sci. Soc. Am. J. 77 (6), 1888–1919.
- Oklahoma Forestry Services. 2010. Oklahoma Forest Resource Assessment. http://www.forestry.ok.gov/Websites/forestry/Images/Oklahoma%20Forest%20Resource% 20Assessment,%20FINAL%20FOR%20WEB.pdf. Accessed 20 November 2019.
- Owe, M., Chang, A., Golus, R.E., 1988. Estimating surface soil moisture from satellite microwave measurements and a satellite derived vegetation index. Remote Sens. Environ. 24 (2), 331–345.
- Patrignani, A., Ochsner, T.E., 2018. Modeling transient soil moisture dichotomies in landscapes with intermixed land covers. J. Hydrol. 566, 783–794.
- Peng, J., Loew, A., Merlin, O., Verhoest, N.E.C., 2017. A review of spatial downscaling of satellite remotely sensed soil moisture. Rev. Geophys.
- Sánchez, N., Martínez-Fernández, J., Calera, A., Torres, E., Pérez-Gutiérrez, C., 2010. Combining remote sensing and in-situ soil moisture data for the application and validation of a distributed water balance model (HIDROMORE). Agric. Water Manag. 98 (1), 69–78.
- Sánchez, N., Martínez-Fernández, J., González-Piqueras, J., González-Dugo, M.P., Baroncini-Turrichia, G., Torres, E., Calera, A., Pérez-Gutiérrez, C., 2012a. Water balance at plot scale for soil moisture estimation using vegetation parameters. Agric. Forest Meteorol. 166, 1–9.
- Sánchez, N., Martínez-Fernández, J., Rodríguez-Ruiz, M., Torres, E., Calera, A., 2012b. A simulation of soil water content based on remote sensing in a semi-arid Mediterranean agricultural landscape. Spanish J. Agric. Res. 10 (2), 521–532.
- Sazib, Nazmus, Mladenova, Iliana, Bolten, John, 2018. Leveraging the Google Earth Engine for Drought Assessment Using Global Soil Moisture Data. Remote Sensing 10 (18), 1265. https://doi.org/10.3390/rs10081265. In press.
- Schnur, M.T., Xie, H., Wang, X., 2010. Estimating root zone soil moisture at distant sites using MODIS NDVI and EVI in a semi-arid region of southwestern USA. Ecol. Inf. 5 (5), 400–409.

- Sun, X., Zou, C.B., Wilcox, B., Stebler, E., 2018. Effect of vegetation on the energy balance and evapotranspiration in tallgrass prairie: a paired study using the eddycovariance method. Bound. Layer Meteorol.
- Sutherland, A., J.D. Carlson, and M. Kizer. 2005. Oklahoma Mesonet Evapotranspiration product description. https://www.mesonet.org/images/site/Evapotranspiration%20 Product%20Description%20Mar%202005.pdf.
- Transtrum, M.K., Qiu, P., 2016. Bridging mechanistic and phenomenological models of complex biological systems. PLOS Comput. Biol. 12 (5), e1004915.
- Wagle, Pradeep, Gowda, P.H., Northup, B.K., 2019. Dynamics of evapotranspiration over a non-irrigated alfalfa field in the Southern Great Plains of the United States. Agric. Water Manag. 223 https://doi.org/10.1016/j.agwat.2019.105727.
- Wagner, W., Blöschl, G., Pampaloni, P., Calvet, J.C., Bizzarri, B., Wigneron, J.P., Kerr, Y., 2007. Operational readiness of microwave remote sensing of soil moisture for hydrologic applications. Hydrol. Res. 38 (1), 1–20.
- Wagner, W., Dorigo, W., de Jeu, R., Fernandez, D., Benveniste, J., Haas, E., Ertl, M., 2012. Fusion of active and passive microwave observations to create an essential climate variable data record on soil moisture. ISPRS Ann. Photogram. Remote Sens. Spat. Inf. Sci. Volume 1-7.
- Wang, X., Xie, H., Guan, H., Zhou, X., 2007. Different responses of MODIS-derived NDVI to root-zone soil moisture in semi-arid and humid regions. J. Hydrol. 340 (1), 12–24.

- Wyatt, B.M., Ochsner, T.E., Fiebrich, C.A., Neel, C.R., Wallace, D.S., 2017. Useful drainage estimates obtained from a large-scale soil moisture monitoring network by applying the unit-gradient assumption. Vadose Zone J. 16 (6).
- Wyatt, B.M., Ochsner, T.E., Krueger, E.S., Jones, E.T., 2020. In-situ soil moisture data improve seasonal streamflow forecast accuracy in rainfall-dominated watersheds. J. Hydrol. 590 https://doi.org/10.1016/j.jhydrol.2020.125404.
- Yimam, Y.T., Ochsner, T.E., Kakani, V.G., Warren, J.G., 2014. Soil Water Dynamics and Evapotranspiration under Annual and Perennial Bioenergy Crops. Soil Sci. Soc. Am. J. 78 (5), 1584–1593.
- Yimam, Y.T., Ochsner, T.E., Fox, G.A., 2017. Hydrologic cost-effectiveness ratio favors switchgrass production on marginal croplands over existing grasslands. PLOS One 12 (8)
- Zhang, Y., Zhao, W., Ochsner, T.E., Wyatt, B.M., Liu, H., Yang, Q., 2019. Estimating deep drainage using deep soil moisture data under young irrigated cropland in a desertoasis ecotone, Northwest China. Vadose Zone J. 18 (1).
- Zou, C.B., Caterina, G.L., Will, R.E., Stebler, E., Turton, D., 2015. Canopy interception for a tallgrass prairie under juniper encroachment. PLOS One 10 (11). https://doi.org/ 10.1371/journal.pone.0141422.
- Zou, C.B., Turton, D.J., Will, R.E., Engle, D.M., Fuhlendorf, S.D., 2014. Alteration of hydrological processes and streamflow with juniper (*Juniperus virginiana*) encroachment in a mesic grassland catchment. Hydrol. Process. 28 (26), 6173–6182.